REPORT DOCUMENTATION PAGE

AFRL-SR-AR-TR-04-

0285

1. AGENCY USE ONLY *(Leave blank)*	2. REPORT DATE	3. REPORT TYPE AND DATES COVERED
	17-JUN-2003	FINAL (1-JULY-1998 TO 31-DEC-2002

4. TITLE AND SUBTITLE
RESEARCH AND DEVELOPMENT ON ASPIRATED COMPRESSORS

5. FUNDING NUMBERS
F49620-98-1-0493

6. AUTHOR(S)
PROFESSOR JACK KERREBROCK

7. PERFORMING ORGANIZATION NAME(S) AND ADDRESS(ES)
MASSACHUSETTS INSTITUTE OF TECHNOLOGY
DEPARTMENT OF AERONAUTICS AND ASTRONAUTICS
CAMBRIDGE, MA 02139

8. PERFORMING ORGANIZATION REPORT NUMBER

9. SPONSORING/MONITORING AGENCY NAME(S) AND ADDRESS(ES)
AFOSR/NA
4015 WILSON BOULVARD
ARLINGTON, VA 22203

10. SPONSORING/MONITORING AGENCY REPORT NUMBER

11. SUPPLEMENTARY NOTES

12a. DISTRIBUTION AVAILABILITY STATEMENT

Approved for public release;
distribution unlimited.

13. ABSTRACT *(Maximum 200 words)*

Overall, the program has comprised three main elements:

1) Development of a computational design system for design of aspirated compressors. This work has been reported in [1.2,3].

1) Design, construction, and test of a low tip speed fan stage incorporating aspiration in both the rotor fan stator. This work has been reported in [6].

1) Design, construction and test of a high tip speed, high-pressure ratio fan stage. The aerodynamic design and analysis of this stage was reported in [2]. Its mechanical design, construction, and test are the main subject of this report.

In summary, the program has succeeded in all of the three elements, yielding a design system that produces compressor designs that incorporate boundary layer control by aspiration, and deliver approximately double the work of conventional stages, with competitive through-flow efficiency. This has been demonstrated experimentally via a low tip speed stage with pressure ratio of 1.6 at a tip speed of 750 ft/sec, and via a high tips speed stage with pressure ratio of 3.2 at a tip speed of 1500 ft/sec. The low tip speed stage was demonstrated in the MIT Blowdown Compressor Facility. The high tip speed stage was demonstrated in a compressor facility at the NASA Glenn Research Center, at full-simulated engine conditions, so that although its primary objective was an aerodynamic verification, it also constituted a proof of feasibility of at least one structural concept for aspirated compressors.

14. SUBJECT TERMS	15. NUMBER OF PAGES
	30
	16. PRICE CODE

17. SECURITY CLASSIFICATION OF REPORT	18. SECURITY CLASSIFICATION OF THIS PAGE	19. SECURITY CLASSIFICATION OF ABSTRACT	20. LIMITATION OF ABSTRACT
UNCLASSIFIED	UNCLASSIFIED	UNCLASSIFIED	

Gas Turbine Laboratory
Department of Aeronautics and Astronautics
Massachusetts Institute of Technology
Cambridge, MA 02139

Final Technical Report on
AFOSR Grant F49620-98-1-0493

entitled

RESEARCH AND DEVELOPMENT ON ASPIRATED COMPRESSORS

submitted to

DARPA/TTO
3701 N. Fairfax Drive
Arlington, VA 22203-1714

ATTN: Dr Richard Wlezien
Dr. Steven H. Walker (AFOSR)

TECHNICAL CONTRIBUTORS:
J. Adamczyk
E. Braunscheidel
A. Epstein, Co-Investigator
J. Kerrebrock, Co-Investigator
A. Merchant
B. Schuler
A. Strazisar
B. Wilson

PERIOD OF INVESTIGATION: July 1, 1998 – December 31, 2002

April 2003

CONTENTS

INTRODUCTION

This Final Technical Report records and summarizes work carried out by the MIT Gas Turbine Laboratory on the project entitled"Research and Development on Aspirated Compressors" over the period from July 1 1998 to Dec 31, 2002. Much of the work has been previously reported by paper presentations and/or publications; these will be cited and summarized but not repeated here in detail. The final phase of the work, consisting of the design, construction, and test of a high-pressure ratio stage, will be reported in more detail.

Overall, the program has comprised three main elements: .

1) Development of a computational design system for design of aspirated compressors. This work has been reported in [1, 2, 3].
1) Design, construction, and test of a low tip speed fan stage incorporating aspiration in both the rotor and stator. This work has been reported in [6].
1) Design, construction, and test of a high tip speed, high pressure ratio fan stage. The aerodynamic design and analysis of this stage was reported in [2]. Its mechanical design, construction, and test are the main subject of this report.

In summary, the program has succeeded in all of the three elements, yielding a design system that produces compressor designs that incorporate boundary layer control by aspiration, and deliver approximately double the work of conventional stages, with competitive throughflow efficiency. This has been demonstrated experimentally via a low tip speed stage with pressure ratio of 1.6 at a tip speed of 750 ft/sec, and via a high tip speed stage with pressure ratio of 3.2 at a tip speed of 1500 ft/sec. The low tip speed stage was demonstrated in the MIT Blowdown Compressor Facility. The high tip speed stage was demonstrated in a compressor facility at the NASA Glenn Research Center, at full simulated engine conditions, so that although its primary objective was an aerodynamic verification, it also constituted a proof of feasibility of at least one structural concept for aspirated compressors.

OVERVIEW OF HIGH PRESSURE RATIO STAGE

The design point of a pressure ratio of approximately 3.4 at a tip speed of 1,500 ft/sec was selected to assess the limit of pressure ratio attainable in a single stage by use of aspiration, within conventional tip speed limits set by structural considerations. To avoid the uncertainties in design and analysis caused by tip clearance flows, a tip shroud was included in the design. This

shroud also enabled the efficient collection of the bleed flow from the rotor blades and its transfer to the casing. The stator was required to fully remove the rotor swirl, producing an axial discharge. It is important to note that although this stage might be thought of as a replacement for two- or three-stage fans, this was not the design intent; rather it was to define the limit of work attainable in a single stage with aspiration.

Early computational design work using the MISES-based MIT design approach, followed by three-dimensional analyses by APNASA(NASA Glenn) and also by Pratt&Whitney's NASTAR code, verified that the rotor should be aerodynamically feasible, and that the stator, while likely to be marginal in efficiency, was also feasible. The design work indicated that bleed fractions on the order of 0.01 to 0.02 would be required for each blade row.

The combination of a high tip speed shroud, very high solidity and camber, and the requirement for somewhat intricate passages in the rotor blades for bleed removal, posed an unusual structural challenge. After consideration of a number of possibilities, an unique structural concept was devised, in which the rotor (and stator) were divided into two parts by a separation plane perpendicular to the rotational axis. The shorter axial length of each of the halves enabled their integral machining from a solid, and also allowed the machining of the suction passages into each half, from the parting plane.

Preliminary stress calculations indicated that the tip shroud would suffer stresses well beyond the limits of the strongest Titanium alloys (*e.g.* Ti 6246), so a graphite-epoxy composite reinforcement was included, wound into circumferential channels in the shroud. By this means it was found that the shroud could be made to be self-supporting, imposing no loads on the blades. The shroud also stiffened the blade, minimizing vibrational and flutter problems. This structural concept was analyzed in detail by Honeywell Aircraft Engines, whose results will be included below, in the discussion of the mechanical design.

The machining of the four bladed discs was performed by Turbocam of Dover, NH. The composite winding was carried out by Wilson Composites of Folsom, CA, using equipment available at Kirtland Air Force Base, NM. This effort was somewhat more troublesome than expected; it is described in detail below. In the end, though, the rotor operated successfully to full design speed without incident.

Installation of this stage in the NASA Glenn compressor facility required extensive modifications and additions, principally because of the need to handle separately several bleed

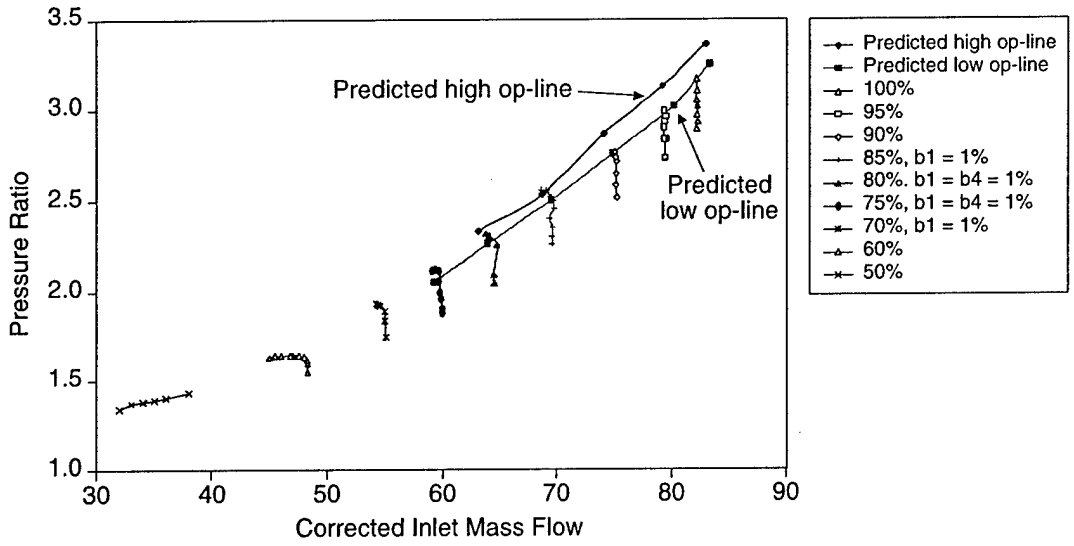

Figure 1: Compressor map, pressure ratio vs corrected mass flow, for high pressure ratio aspirated compressor; 50-85% speedlines are choke to stall, 90-100% speedlines are choke to low op-line PR.

flows. These included one on the casing upstream of the rotor, two from the rotor tip via the shroud, one on the casing ahead of the stator, one at the hub of the stator, one from the stator suction surface, and a starting bleed at the stator hub. This work will be summarized below.

The stage was operated during December 2002, yielding the performance depicted in the compressor map of Figure 1. As can be seen from the map, the experimentally determined performance is virtually identical to that predicted computationally, and in turn to the original design intent. The adiabatic efficiencies achieved on the low and high operating lines are shown in Figure 2. For reasons explained below the high operating line was not extended to full design speed.

We take these results to be a validation of both the concept of aspiration and equally important, of the design system.

AERODYNAMIC DESIGN AND ANALYSIS

This section briefly describes 1) the design system and aspirated blade design, 2) aerodynamic design of the stage, and 3) design point and off-design CFD analyses of the stage.

Design System:

The unusually high blade loading and high Mach numbers of the aspirated compressor

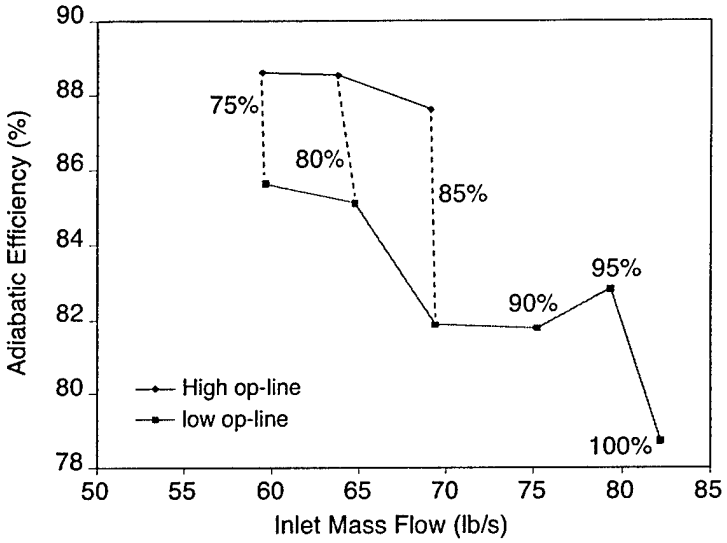

Figure 2: Efficiencies on the low and high operating lines.

stage required a fresh look at the blade design system as well as the design philosophy. These are described in Merchant [3].

Traditional aerodynamic design systems rely on the streamline curvature method, which solves radial equilibrium combined with the energy equation. This approach is not numerically robust and accurate for highly-loaded compressors, with high subsonic through-flow Mach numbers, and strong coupling between the blades and the flowpath. The blade row information in the streamline curvature method is typically modeled using camberline angles and a fixed thickness distribution. Losses, flow angle deviation, and blocakge are supplied via empirical relations.

The design system assembled for designing the highly-loaded aspirated compressor consists of an axisymmetric throughflow solver coupled with the quasi-3D blade-to-blade solver MISES [4]. Figure 3 shows the layout of the design system. In contrast to traditional systems, the present system provides at least two important advantages. 1) The throughflow solver used in the present design system solves the complete axisymmetric Euler equations, providing a more accurate throughflow solution of the compressor. In addition, the streamline variation within the blade rows is also more accurate. 2) The quasi-3D MISES solver provides accurate and up-to-date blade-to-blade information to the throughflow solver as the blade shape evolves in the design process.

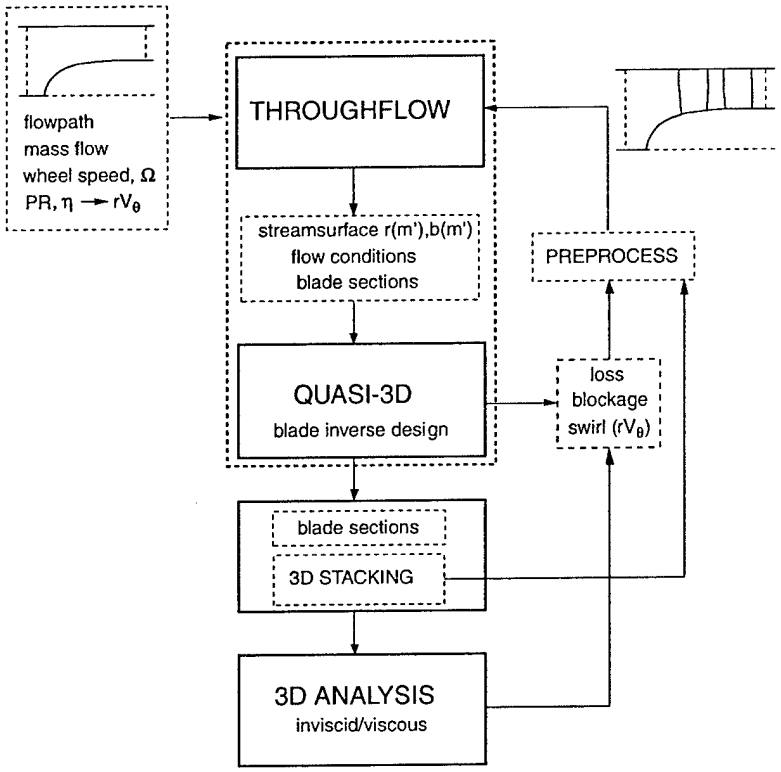

Figure 3: Aerodynamic design system.

This combination of the fully axisymmetric solver combined with MISES results in a significantly more accurate and robust design system than traditional aerodynamic design systems. In addition, the inviscid-viscous formulation and inverse design features in MISES provide unprecedented flexibility in designing advanced aspirated blade sections. The boundary layer formulation in MISES was modified to include a suction model which makes the suction calculation an integral part of the blade design procedure.

The effect of endwall boundary layers, spanwise mixing, and non-axisymmetric effects, which require additional modeling and empirical input, were not directly included in the through-flow calculation in the initial design iteration. However, blockage and losses obtained by post-processing the 3D viscous analysis were used to refine the design in subsequent iterations.

Blade Design

The critical design features that distinguish aspirated blades from conventional blades are: 1) blade thickness, 2) smooth leading edge shape, 3) supersonic precompression, 4) blunt

diverging trailing edge, and 5) pressure side shape. Each feature is briefly discussed below.

1) Aspiration places a severe constraint on the blade thickness, which has to be sufficient to accommodate the suction passages inside the blade as well as meet structural requirements. Aspirated blades have at least two times the maximum thickness of typical conventional blades designed for a similar flow regime. The location of the maximum thickness is therefore critical in achieving good performance, especially for transonic and supersonic blades, where the blade thickness can have a significant impact on the shock losses.

2) The thickness requirement on aspirated blades also constrains the thickness of the leading edge region. Therefore, considerable attention has to be given to the design of the leading edge region to achieve good performance. A poorly designed leading edge region may result in regions of overspeeds and spikes in the pressure distribution. This may cause local separation of the flow resulting in higher losses and lower useful incidence range. The local separation may be particularly detrimental for supersonic blades that are sensitive to blockage. A distinctive characteristic of the aspirated blades designed at MIT is the smooth pressure distribution on the suction and pressure sides near the leading edge region. In contrast, spikes in the pressure distribution of conventional supersonic compressor blades are unavoidable due to leading circles or ellipses that are used to close the blade shape.

3) Precompression lowers the Mach number before the terminal passage shock through a series of weak compression waves. Judicious use of precompression on the supersonic aspirated blades increased the subsonic loading capability, increased the efficiency, and lowered the bleed requirement. Excessive precompression, where the flow is decelerated to nearly sonic conditions has, in early supersonic compressors, resulted in unsuccessful designs that have not achieved design mass flows. The position of the suction slot at the throat of the blade passage is also beneficial since bleeding the flow increases the throat margin. Numerical studies at off-design conditions have shown that aspiration delays the "spilling" of the passage shock as the blade loading is increased.

4) The blunt diverging trailing edge concept has been used to increase the aft loading of aspirated blades. In addition to increasing the aft loading, another advantage of this concept is that the pressure gradient on the suction side can be relaxed close to the trailing edge, and the flow deviation (difference between the blade metal angle and flow angle) can also be significantly reduced. The trailing edge thickness controls the loading increase that can be

obtained, but also has the potential of increasing the profile loss due to the base pressure. Therefore, the effectiveness of the diverging trailing concept has to be weighed against the overall performance of the blade. The criteria used to determine trailing edge thickness for aspirated blades are: 1) the boundary layer remains attached up to the trailing edge, and 2) the trailing edge thickness does not exceed the boundary layer displacement thickness.

5) Design of the pressure surface shape, although usually determined by structural constraints, requires special attention in the case of aspirated blades. While pressure side separations occur on high turning turbine cascades, conventional compressor blades are limited by separation of the suction side boundary layer. The large turning combined with relatively high inlet Mach numbers of aspirated blades can lead to severe adverse pressure gradients on the blade pressure side. The impingement of the passage shock on the pressure side may also lead to separation of the pressure side boundary layer. This occurs at the rotor tip and stator hub of the aspirated high-speed stage.

Stage Aerodynamic Design

The aerodynamic design of the high-speed stage involved a preliminary design phase where the flowpath and meridional geometry of the stage were developed. This was followed by design iterations using the complete design system described above to develop the full 3D blade geometry. The primary aspiration requirement on the blade suction side was an outcome of this process, while additional aspiration on the hub and shroud surfaces was determined from the 3D viscous analysis.

The high-speed stage design parameters representing the design intent are presented in Table 1. The diffusion factors are calculated using Lieblein's definition.

Bleed Configuration and Requirements

A schematic of the boundary layer suction or bleed configuration that was used in the computational design and analysis is shown Figure 4. The corresponding bleed requirement for each bleed location is given in Table 2. The bleed mass flow is reported in percent of the stage inlet mass flow. The slot arrangement consists of primary bleed slots in the spanwise direction on the blade suction surfaces, and secondary bleed slots in the circumferential and chordwise directions. The rotor spanwise slot extends from 40% span up to the tip, and the stator spanwise slot extends from hub to tip. The circumferential slots on both blade rows extend over the entire

Table 1: High Speed Stage Design Parameters

Tip Speed	1500 ft/s (457 m/s)
Stage Pressure Ratio	3.5
Stage Mass Flow / Area	42.5 lbm/s-ft^2
Rotor face Axial Mach No.	0.65
Stage exit Mach No.	0.5
Rotor Tip Rel. Mach No.	1.5
Stator Hub Abs. Mach No.	1.5
Max. Diffusion Factor. (rot/sta)	0.76 / 0.68
Tip Blade Loading ($\Delta H/U^2$)	0.7
Rotor Inlet (r_{hub}/r_{tip})	0.40
Stator Exit (r_{hub}/r_{tip})	0.81
Blade Count (rot/sta)	26 / 31
Rotor Tip Solidity	2.14
Stator Hub Solidity	2.95

blade pitch, and the final locations and bleed requirements of these slots were determined iteratively from the 3D viscous calculations. The chordwise slot near the stator hub suction surface was added to control the excessive separation and growth of secondary flow developing along the stator hub predicted by the 3D viscous calculation. This slot extends from 25% to 75% chord.

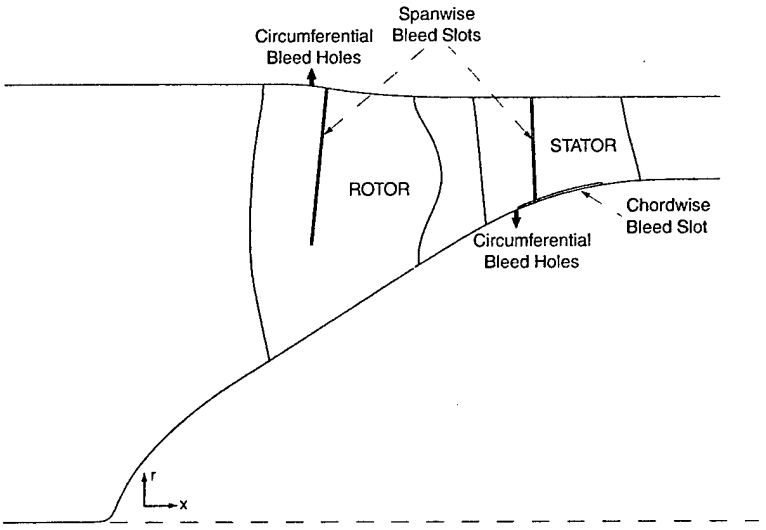

Figure 4: Bleed configuration.

Table 2: Stage Design Bleed Requirement

Blade Row / Slot Type	Bleed Mass %
Rotor circumferential slot	1.0
Rotor spanwise slot	2.0
Stator circumferential slot	1.0
Stator spanwise slot	2.0
Stator chordwise slot	1.0

Flowpath and Blade Design

In contrast to conventional compressors, the flowpath of the high-speed stage is strongly coupled to the blade design and has a significant impact on the overall stage performance. The hub ramp across the rotor was selected to obtain a reasonable axial velocity ratio at the rotor meanline and at the same time to minimize the Mach number entering the stator. The hub profile is parabolic in shape upstream of the rotor and varies linearly across the rotor. The hub ramp angle is 33° across the rotor and approximately 12° across the stator. The tip radius is decreased across the rotor contracting the flowpath area by an additional 5% in order to lower the static pressure rise across the rotor, and consequently to relieve the excessive growth of the shroud boundary layer. The shroud flowpath profile is also shaped to provide some pre-compression of the flow near the rotor passage shock impingement location.

The blade sections for the high-speed stage embody the design features discussed above. The best illustration of the design philosophy is the rotor tip section, which is also one of the most critical sections of the stage.

Figures 5 and 6 show the rotor tip section isentropic Mach number distribution and blade-to-blade contours of Mach number. The peak total pressure ratio for this section is 3.7. The diffusion factor is 0.76 and is the maximum for the rotor. The leading edge is shaped to provide a smooth transition from the leading edge region to the suction and pressure sides. The blade suction side from the leading edge up to mid-chord is shaped to pre-compress the flow just before the passage shock. The suction slot is located just downstream of the shock and tends to hold the foot of the shock at the slot location. The pressure surface shows a fairly strong adverse pressure gradient up to 40% chord followed by a constant Mach number section up to the trailing edge. The blade pressure surface was shaped to weaken the passage shock impingement thus minimizing the boundary layer growth in this region. The effectiveness of the diverging trailing

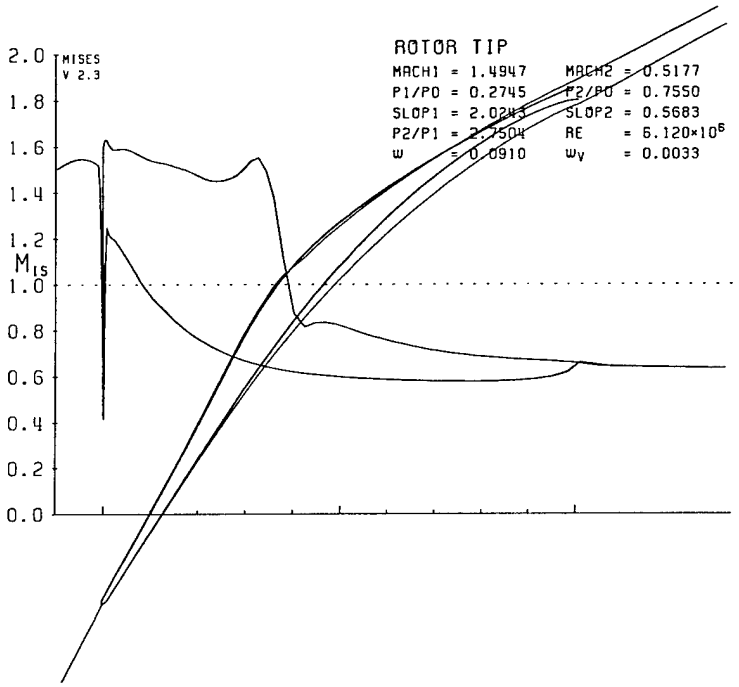

Figure 5: Rotor tip section isentropic Mach number profile.

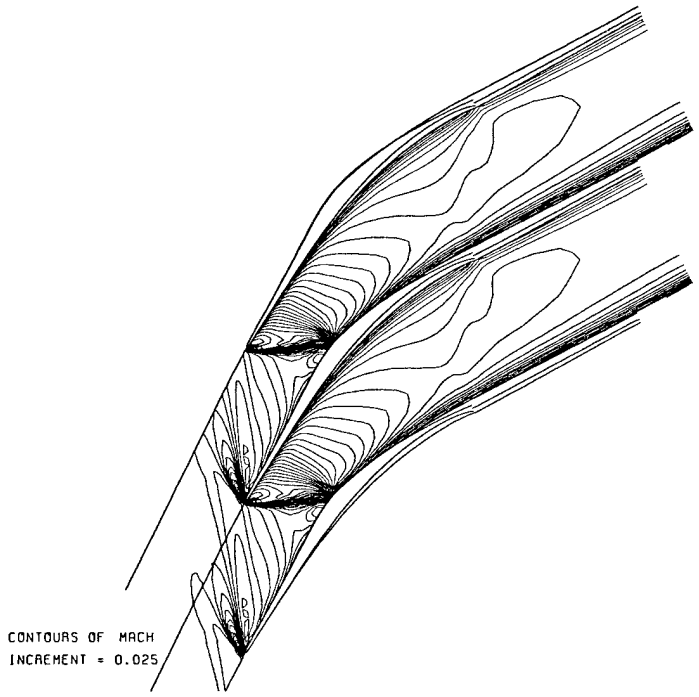

Figure 6: Rotor tip Mach number contours.

edge in increasing the blade loading is diminished due to the unusually thick pressure side boundary layer.

The blade-to-blade contours of Mach number in Figure 6 show that the passage shock coalesces with the bow shock just downstream of the maximum thickness location. The effect of shaping pressure surface to weaken the passage shock is seen downstream of the leading edge on the pressure side. A significant portion of the blade is devoted to subsonic turning, which is required to achieve the design pressure ratio. The blade thickness and leading edge radius are considerably greater than those of conventional supersonic blades designed for the same inlet Mach number.

Figure 7 shows the shape parameter (H_k) distribution and boundary layer profiles on the blade suction surface for the tip. The shape parameter on the suction side is almost constant in the pre-compression region and undergoes an increase across the shock followed by a growth in the pressure recovery region. The effect of aspiration in controlling the rapid increase in H_k is clearly seen. Figure 8 shows the effect of aspiration in decreasing the displacement (δ^*) and momentum thickness (θ), which are indicators of flow blockage and viscous loss in the rotor.

3D Viscous CFD Analysis

The 3D viscous analysis of the stage was carried out using the APNASA multi-stage code developed by Adamczyk [5]. The multi-stage average passage model in the code enables an

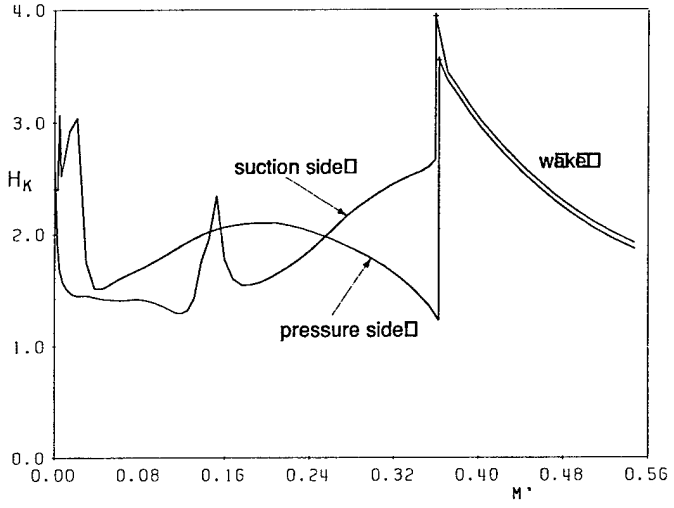

Figure 7: Rotor tip shape parameter profile.

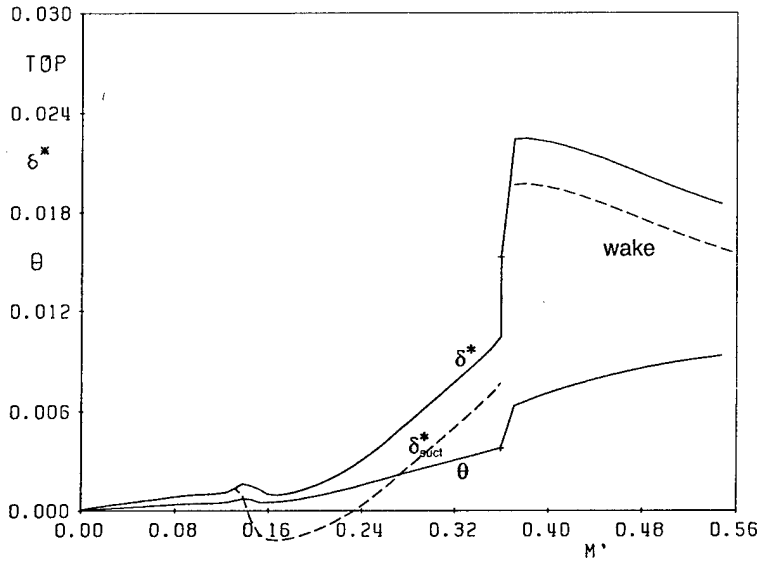

Figure 8: Displacement and momentum thicknesses for rotor tip section.

accurate calculation of the interaction between blade rows. This was critical in the analysis of the high-speed stage due to the high supersonic Mach numbers entering the stator and the very high blade loading . The computational mesh used for the analyses has 199 axial, 51 circumferential, and 51 spanwise grid points. The code was modified with a simple transpiration boundary condition on the blade and flowpath surfaces to model suction.

Design Point Performance

Evaluation of the stage using three-dimensional calculations predicted a peak adiabatic efficiency of 86%, and a peak pressure ratio of 3.4. The rotor achieved peak pressure ratio of 3.7 and a peak efficiency of 93%. These are indicate the mass averaged throughflow performance. The loss in performance of the stage can be attributed primarily to the stator performance. Despite the fact that the blade design was carried out using a quasi-3D approach, the performance predicted by the three-dimensional calculations was found to be in good agreement with the design intent. The exception was near the rotor tip and stator hub where the flow behavior was strongly influenced by the endwall boundary layers.

Figure 9 shows the contours of Mach number of a rotor section at 95% span. The shock position is in agreement with the quasi-3D calculation, and the effect of suction at the foot of the passage shock can be seen in the plot. The rotor shows a region of low-momentum fluid in the

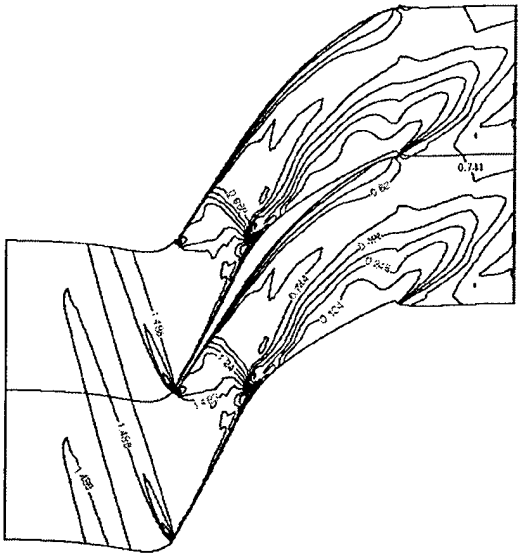

Figure 9: Rotor Mach number contours at 95% span, from APNASA.

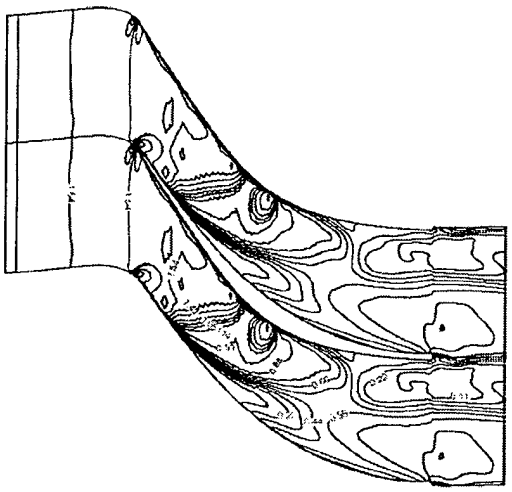

Figure 10: Stator Mach number contours at 10% span, from APNASA.

subsonic section of the passage due to interaction with the shroud boundary layer. The radial extent of the low momentum flow on the rotor suction side can be seen in Figure 9. At lower span sections the boundary layer was well attached due to aspiration, resulting in relatively thin wakes and high efficiency.

Figure 10 shows the contours of Mach number of a stator section at 10%. The flow conditions near the stator hub were far more severe than the rotor tip due to the high inlet Mach of 1.5 combined with a total flow turning of 60 degrees. The effect of the bleed can be seen on

the suction side just downstream of the passage shock. The impingement of the passage shock on the pressure surface of the stator and the high level of diffusion initiates a corner separation, which then migrates toward the suction side as well as grows radially. The extent of the separation can also be seen in Figure 9. The chordwise slot aspirating 1% of the flow was used to alleviate this separation.

Off-design Performance

An off-design study along the operating lines was performed in order to assess the performance of the stage at lower blade speeds and to develop a test plan for the experiment. CFD analyses were carried out at fixed exit corrected mass flows, which implies a fixed throttle setting, at different RPMs. This was carried out at a high operating line close to stall and a low operating sufficiently away from stall.

Figure 11 shows the pressure ratio performance of the stage and Figure 12 shows the efficiency of the stage along the operating lines. The stage does not stall along either operating line at lower blade speeds. The rotor efficiency remains above 90% over the entire speed range. The stage efficiency shows an increase at lower blade speeds with peak efficiencies of 87% at the high operating line and 85% on the low operating line. The different behavior of the rotor and stage efficiencies indicates the impact of the stator loss on the stage performance. It is also

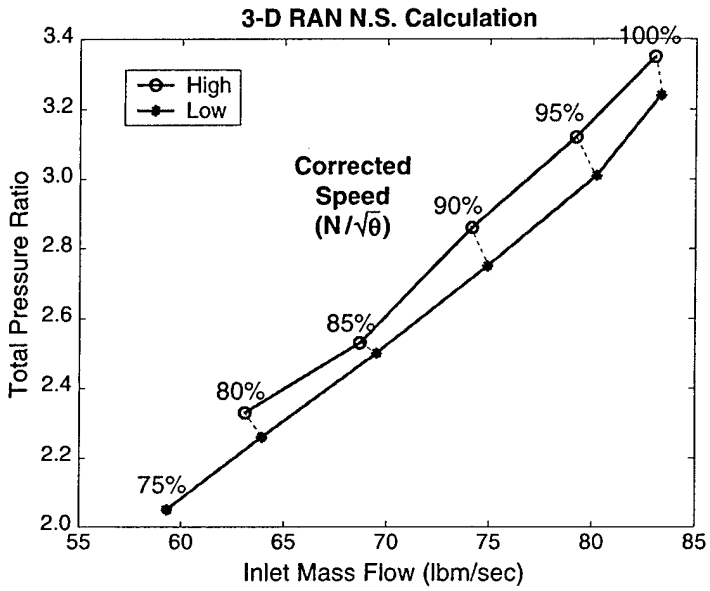

Figure 11: Computed pressure ratios on low and high operating lines.

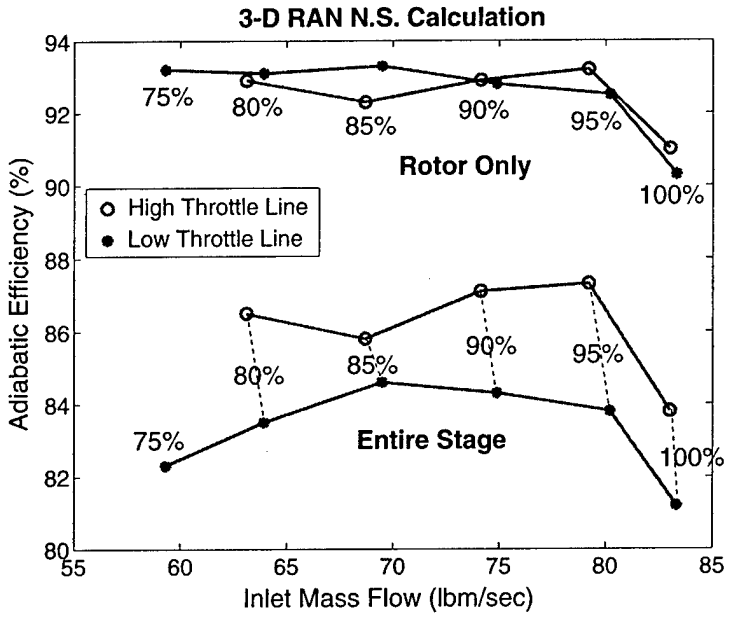

Figure 12: Computed efficiency on high and low operating lines.

interesting to note the increase of 3% when the speed is decreased from 100% to 95%. Figures 13 and 14 illustrate the changes in the rotor tip and stator hub flowfields accompanying the speed change.

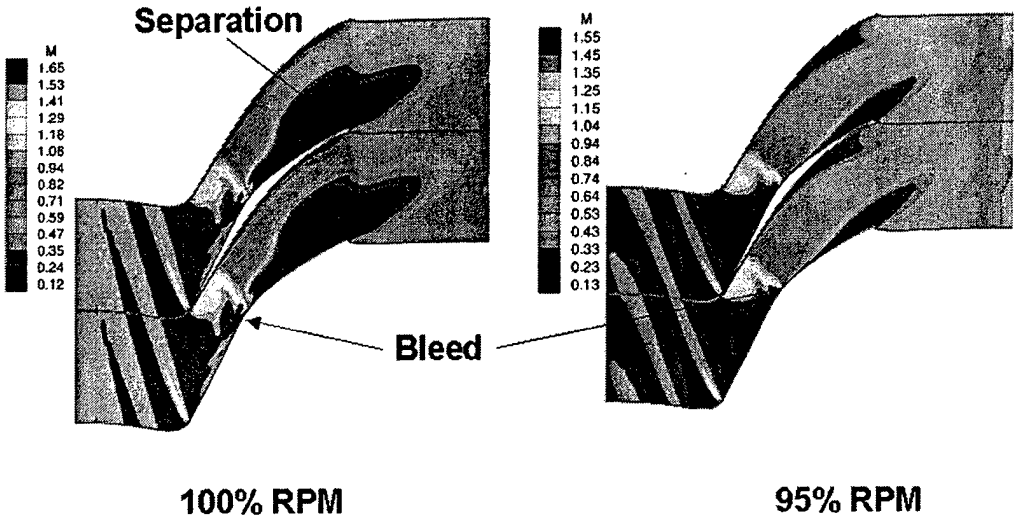

Figure 13: Rotor tip span flow field Mach numbers at 100% and 95% RPM.

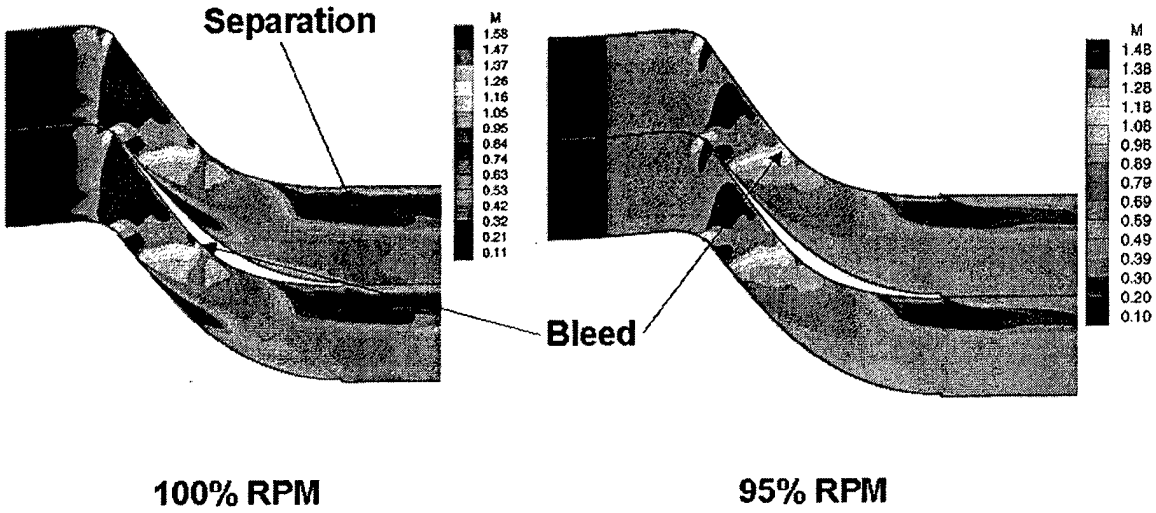

Figure 14: Stator hub span flow field Mach numbers at 100% and 95% RPM.

Bleed Sensitivity Study

The sensitivity of the stage performance to aspiration was studied at 90% of the design RPM. Table 3 summarizes the results of the study, which shows an acceptable decrease in performance at significantly lower bleed fractions. The values in parentheses indicate design conditions.

Table 3: Aspiration Sensitivity at 90% RPM

	Bleed %	PR	Efficiency %	Inlet Mass Flow (lbs/sec)
Rotor	1.1 (2.4)	2.9 (3.0)	90 (93)	-
Stage	2.9 (6.9)	2.7 (2.8)	83 (84)	70 (75)

The aspiration fraction was decreased by more than a factor of two resulting in a 2% decrease in rotor and stage pressure ratios and a 6% decrease in stage inlet mass flow. The rotor efficiency decreases by 3%, but the overall stage efficiency decrease is 1%.

MECHANICAL DESIGN OF STAGE

The overall design of the stage was aerodynamically controlled, so that the mechanical design became a matter of devising a configuration that would meet the mechanical requirements, while providing the shape and tip speed capability dictated by the aerodynamic

design. This is a different logical structure than is usual for compressor stages, where the structural considerations generally play a larger role in the overall design optimization. It was deemed appropriate because the main purpose of the experiment was to assess the viability of aspiration from the aerodynamic standpoint. As noted in the Summary, the desire for as clean an aerodynamic design as possible lead to the use of a tip shroud, to eliminate the tip vortices that result from unshrouded blade tips. In addition, the tip shroud was attractive as a means for transferring the aspirated flow from the blades to the rotor housing.

Taken together these aerodynamically dictated features posed an unusual set of constraints for the mechanical design of the rotor in particular. Preliminary calculations showed that the blade stresses due to the high tip speed and large camber and twist of the blades, were so high as to be unacceptable except for the highest strength/weight titanium alloys, such as Ti-6246, which are not weldable, so a welded structure was ruled out. The calculations also indicated that the shroud, at the design tip speed of 1,500 ft/sec was beyond its self-supporting limit, and given the already high stresses in the blades, it was not feasible to carry much of the centrifugal load of the shroud on the blades. This lead to the decision to use a graphite-polymer composite winding on the shroud, to make it essentially self-supporting. The amount of composite was chosen so that the radial growth of the shroud would match that of the blade tips (without the shroud), so there would be only local radial load transfer from the blade to the shrouds. The shroud does however greatly stiffen the blades torsionally, in the tip region, essentially eliminating flutter issues, and potential problems due to the bleed passages in the blades.

This left the provision of these bleed slots and passages for the aspirated flow as the main remaining problem. Since welding was ruled out for the Ti-6246, it was necessary to machine the bleed passages from the solid. To make this possible and also to facilitate the machining of the blade shapes, it was decided that the rotor disc should be divided on a plane perpendicular to the axis of rotation, into forward and aft portions. The suction passages could then be machined into the two halves, from the separation plane. In assembly the two halves would be bolted together at the periphery and at the hub.

Honeywell Aircraft Engines was sub-contracted to carry out the detailed design and analysis of the stage along these lines. A full report of their findings is available [5], while some

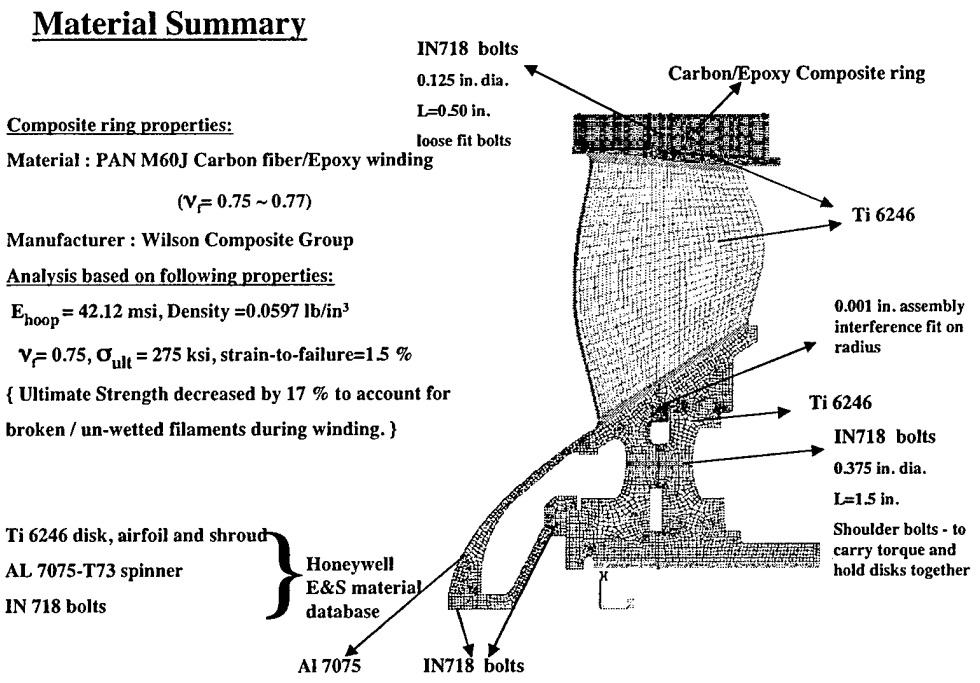

Figure 15: Rotor structural concept, showing fore and aft integrally bladed halves, with composite wound tip shroud.

of the key results will be summarized here. The structural concept of the rotor is illustrated in Figure 15.

As can be seen the composite winding of the shroud was implemented as three rings in channels in the titanium shroud, the division of the front ring being to separate two of the rotor bleeds. The rotor is mounted on the shaft by means of a polygon, which transmits torque and is self-centering when the bore expands at speed. The bleed flow was carried through flanges between the composite rings. Drawings of the front and aft portions of the rotor showing the suction passages, are in Figures 16 and 17. The aspirated flow was taken from the suction surface of the blade through slots, into the radial passages and discharged from the tip at an angle of 45 degrees, backward to the rotation. This was to minimize the pumping work for the bleed flow, and thereby the temperature of the aspirated flow.

The equivalent stresses in the blades computed by Honeywell are shown for the suction and pressure sides in Figures 18 and 19. As can be seen the stresses are locally very close to the allowable for Ti-6246, which we set at about 120,000 psi. On the other hand the average stresses are well below the limit.

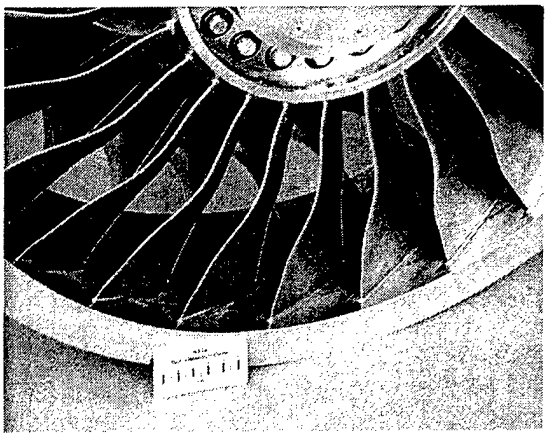

Figure 16: Front view of rotor,.

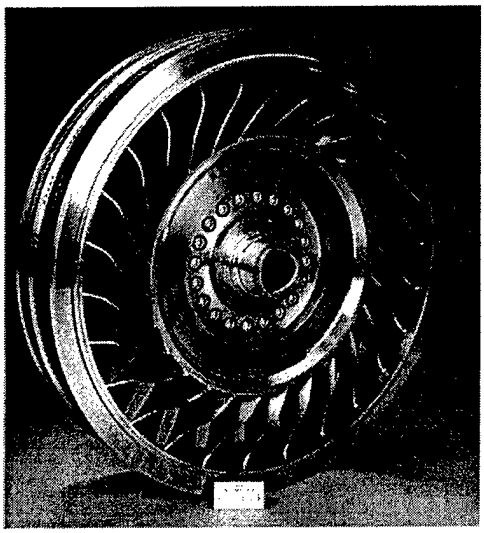

Figure 17: Rear view of rotor.

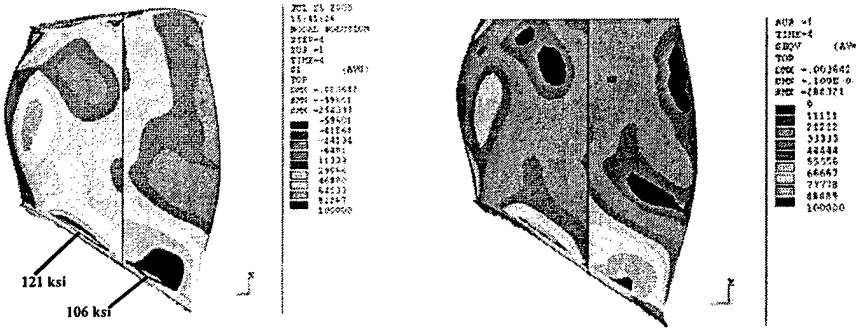

Figure 18: Equivalent stresses in rotor on suction surface.

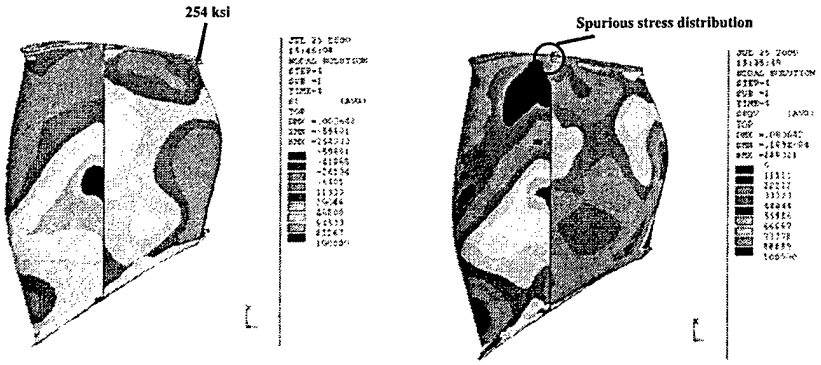

Figure 19: Equivalent stresses in rotor on pressure surface.

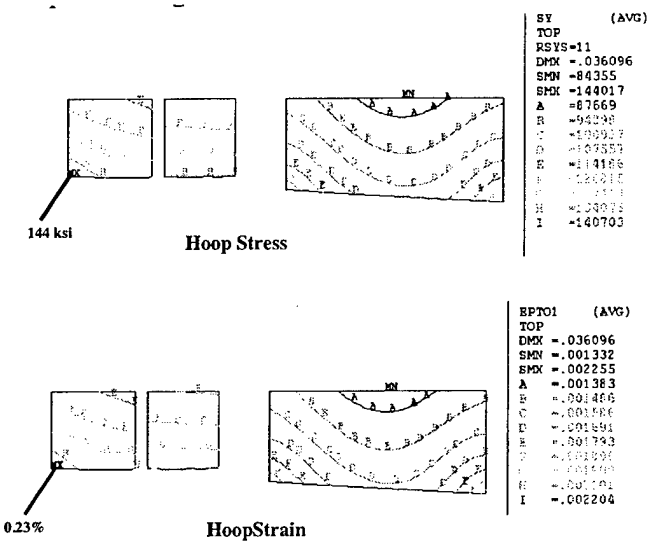

Figure 20: Stress distribution in composite support rings for shroud.

The stresses computed for the composite rings are shown in Figure 20. Here the maximum was about 144,000 psi. Estimates of the allowable stress for the composite varied somewhat depending on the degradation assumed from the values computed from the fiber-polymer mix. Hydrostatic testing of two rings that simulated the winding later indicated an ultimate strength for the composite of about 200,000 psi, so based on this measured value and the computed maximum, the design had about a 40% margin. In the event it did operate satisfactorily at design speed.

TEST FACILITY MODIFICATIONS AND STAGE TESTING

Summary

This report presents the results from the experimental evaluation of the aspirated compressor. The stage was tested with rotor speeds at 50 to100 percent of design speed. Overall performance was obtained by arrays of pressure and temperature rakes downstream of the stage. Speedlines were obtained from choke to near stall up to 85 percent of design speed. At speeds above 85 percent, the speedlines were obtained from choke to a predetermined low operating line for which a predicted point existed. At the design tip speed of 1500 ft/s the measured overall pressure ratio was 3.17 with a corresponding adiabatic efficiency of 78.7%. This condition compared favorably with the predicted low operation line operating point.

At design speed, the total stage bleed rate was 3.5%, which is roughly half of the intended bleed rates. During the course of testing, all bleeds were turned off and the stage immediately stalled, confirming that bleeds were required to successfully operate the stage.

Apparatus and Procedure

Table 4: Test Stage

Stage features:	
Tip shrouded rotor	
Fixed stators	
Bullet nose spinner	
Cantilevered bearing housing design	
Total Pressure ratio	
Rotor	3.8
Stage	3.4
Tip diameter, in	20.7
Tip speed ft/s	1500
Rotative speed, rpm	16,607
Weight flow, lb/s	84
Hub-to-tip ratio	0.4
Solidity	
Rotor tip	2.14
Stator hub	2.95
Number of blades	
Rotor	26
Stator	31
Rotor Bleed rate, % of inflow	3
Stage Bleed rate, % of inflow	7

Test Package

The aspirated compressor test package consisted of the rotor and stator, a specially-designed casing to accommodate sealing the rotor bleed flows from the core flow and to collect high swirl flow from the rotor shroud. Seven independently-controlled and metered boundary layer bleed systems were also key elements of the system. These consisted of an inlet boundary layer bleed slot approximately 1 chord upstream of the rotor (B1), a bleed line for the rotor shroud and outer blade slot (B2), rotor blade inner bleed slot (B3), an interstage bleed slot located at the casing (B4), an interstage slot on the hub flowpath (B6), a bleed for the stator blade suction surface(B5), and a final bleed for the stator hub area which covered both pitchwise and chordwise bleed areas (B7) (Figure 21). B4 and B6 were not modeled in the aerodynamic

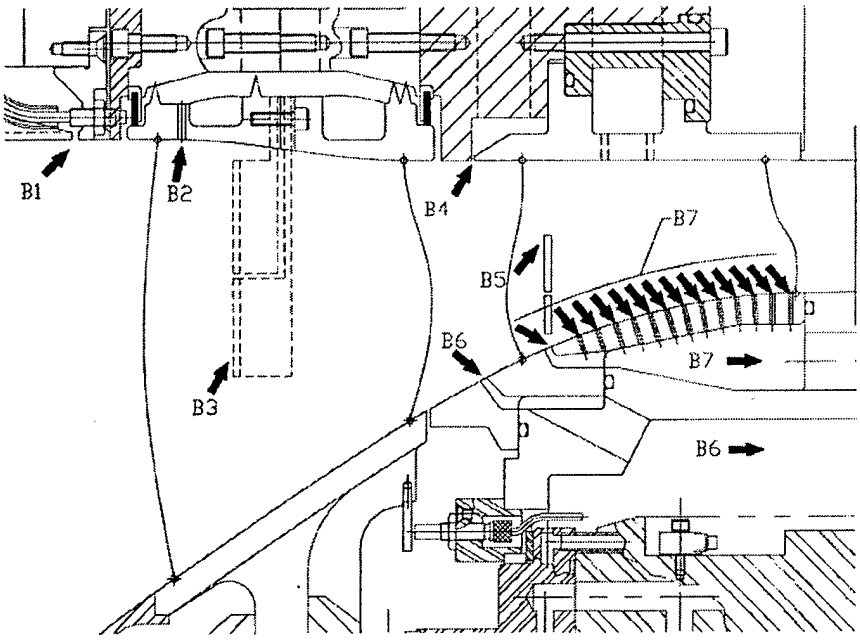

Figure 21: Bleed locations and designations.

analysis or design of the stage, but were added as starting bleeds to insure that the stage could be started. B6 did not have a major effect on the stage, but B4 was required to get the stage above 75% speed, as will be discussed later.

The bleed exhaust system was designed to keep the rotor and stator bleed slots operating in a choked condition. To achieve this condition, a vacuum source was used for all the bleed lines, and all the bleed lines were oversized to insure enough system capacity.

Test Facility

The Glenn Research Center Multistage Compressor Test Facility including a 15,000 hp drive motor and a 5.21:1 gearbox was used for this test effort. The majority of the facility was not modified for this test which used the existing driveline including bearing housing, and air supply and exhaust systems. Two main modifications for this test involved a new inlet and bleed system. The inlet is a bell mouth that transitions the incoming flow down to the 20.7 inch fan diameter. The requirement for multiple bleeds resulted in the addition of seven boundary layer bleed lines. Each bleed line consisted of four to eight inch piping, a straight flow measurement section, and a butterfly valve. Each flow measurement section of piping was calibrated in the

GRC flow lab prior to installation. Each bleed line mass flow was remotely controlled by a butterfly valve downstream of the flow measurement station. In the event of a failure or stall condition, all valves are returned to wide open conditions. The bleed system was tied into the exhaust system that is capable of operating at 2.5 psia while accommodating up to 100 lb/s of flow. This is the same system that the main compressor exhausted to, tie-ins are achieved at different locations to isolate any potential pressure feedbacks.

Inlet air can be provided from a compressed air system that allows dry air to be supplied to the compressor, or air can be pulled from outdoors through a set of filters by the compressor. The outdoor atmospheric air inlet was used for this test program, and due to the Cleveland winter, providing a chilled air system, at no cost, helping to keep the mechanical speed down during the testing. Due to the pressure drop across the main flow measuring orifice, the inlet pressure to the compressor was about 10 psia at the design flow condition, which reduced risks by reducing structural loading of the compressor.

Instrumentation

The state of the facility health was constantly monitored during operation. Health measurements included pressures, temperatures, flow rates, rotor radial and axial proximity, and vibration levels. These were recorded along with the research data. Dynamic pressure measurements and vibration levels were also recorded in real time using a DATAMAX[1] digital data system to enable post analysis if needed.

Inlet airflow was determined from an upstream ASME orifice. The majority of the pressures were measured with an electronic pressure system, other pressures were measured with individually calibrated transducers. Temperature measurements were made using a calibrated system.

The performance of the stage was determined by an array of total pressure and total temperature rakes one chord downstream of the stator, rake designs were chosen that have a wide acceptance flow angle to give accurate measurements at a fixed orientation. The temperature rakes were calibrated for temperature recovery vs. Mach number. The rakes provide seven spanwise measurements at six pitchwise locations, for a total of 42 measurements at the stage exit. Wall statics were the only instrumentation located between the rotor exit and stator inlet, no stator leading edge measurements were available.

Dynamic pressure measurements were obtained from the flow path casing about one chord upstream of the rotor, and were used to detect stall.

Pressure and temperature measurements near the labyrinth teeth rub areas were installed to monitor the shroud condition, and an infrared thermocouple was installed to directly monitor the temperature of the composite material on the rotor. Radial proximity probes monitored the relative gap between the casing and the rotor shroud, to assist in determining if the rotor was growing as predicted.

No strain gage instrumentation was installed on the test package.

Test Procedure

Data was taken for rotative speeds ranging from 50 to 100 percent of design speed. Up to 85 percent, the stage performance was mapped from choke to stall. Above 85 percent, the stage was performance mapped from choke to an operating point that had about a 4% stall margin, these points are referred to as the low operating line. Initially all bleeds were wide open, then bleeds were adjusted to more closely reflect the design intent of the stage. (This mainly involved the starting bleed provisions incorporated into the rig but not accounted for in the analysis.)

The standard method to start the facility was as follows: the exhaust system was energized and all bleed lines opened. The rotor is spun up to a low speed, then the inlet valve is slowly opened to 100 percent. The throttle valve is set to insure that the stage is choked and the rotor is brought up to a maximum speed of 70%. To proceed above 70%, the speed is incrementally increased in 500-1000 rpm steps to allow the thermal growth of the casing to catch up with the radial growth of the rotor. As thermal equilibrium is achieved, additional speed steps are taken. For speeds above 80%, it took about 1/2 hour for a 5% speed change. Thermal equilibrium is required to minimize mechanical interferences that effect labyrinth tooth life, and aerodynamic performance. The rotor is designed for the labyrinth teeth to contact the casing rub strips at 70% speed at an estimated casing temperature. Accelerating too fast could melt the labyrinth teeth resulting in excessive leakage bleed flows, cause local over heat the composite, or induce vibration levels resulting in structural failure.

The exit throttle valve was controlled to achieve the desired pressure ratios at each speed of interest.

Data Reduction Procedure

Orifice weight flow, total pressures, rotative speeds, and temperature were all corrected to standard day conditions based on plenum conditions. The Mach number at each rake port was determined by a linear interpolation of the inner and outer flowpath walls static pressures and the total pressure obtained from that rake port. The pressures were energy averaged, and the temperatures were mass averaged to obtain the overall values presented in Table 4. Overall efficiency was calculated from these overall integrated values of total pressure and total temperature. The calculated efficiencies are for the throughflow, so do not take into account the impact of the bleed that is removed from the flow, on the overall system efficiency.

Results and Discussion

The overall stage performance is given in Figures 1 and 2. The total pressure ratio is plotted as a function of weight flow. The performance curves are typical of a transonic fan for speeds above 60% of design speed, having vertical characteristics. Predicted performance of the stage was executed using APNASA, at peak performance conditions (high operating line), and at a lower operating line. The analysis did not take into account any inlet boundary layer bleed (B1), or interstage starting bleeds (B4, B6), so divergences from predictions must take into account the state of these bleeds. Data for the choke, low and high operating lines are presented in table 4 for 75-85 percent of design speed conditions, and for choke and low operating line conditions for 90-100 percent design speed conditions.

50, 60, and 70% Speedlines

The fifty percent speedline had the inlet boundary layer bleed, B1 was set to 1% of stage core flow at that speed, all other bleeds were flowing at their individual maximum capacities (wide open). At this speed it was very difficult to determine the stalling flow rate.

At sixty percent speed, B1 was set to 1%, interstage starting bleeds (B4 and B6) were turned off, and all other bleeds were at maximum. The stall point was ill defined, as indicated by the measurements.

At seventy percent speed, it was possible to operate with the same bleed setup as for 60%. A peak pressure ratio of 1.93 at 54.2 lb/s flowrate, and adiabatic efficiency of 89%. The stage exhibited a crisp, well defined and repeatable stall point, and the characteristic was nearly vertical. The total mass flow range for this speed was 1 lb/s.

75, 80 and 85% Speedlines

Prior to stepping up to the next speed condition, all bleeds were opened to avoid any unknown instabilities of the stage. After bringing the rig up to 75% speed, B6 (hub starting bleed) was successfully closed, but attempts to close B4 (casing starting bleed) stalled the stage. B4 was reset to 1% of core flow, and the data was taken. The only converged APNASA solution available was for the low operating line, and our measurements matched closely to the predicted pressure ratio. Our slightly higher flow rate was due to B1 and B4 being active which were not accounted for in the simulation. Peak pressure ratio was 2.12, at 59.4 lb/s, and adiabatic efficiency was 88.6%.

The stage behaved similarly at 80% speed, with the stage stalling if B4 was closed from 1% to about 0.25%. The stall induced by closing B4 was not recoverable by opening the throttle valve, but did respond quickly to opening all the bleeds. Speedlines were taken at 80% with the inlet boundary bleed set to 1%. A peak pressure ratio of 2.32 at 63.7 lb/s and adiabatic efficiency of 88.5% were achieved.

Several points were also taken with the inlet boundary layer bleed off, the effects can be seen in Figure 22. At similar pressure ratios the efficiency of the stage with inlet boundary layer bleed on is about 1.2% higher and reduces the stage mass flow rate by 1.3 lb/s.

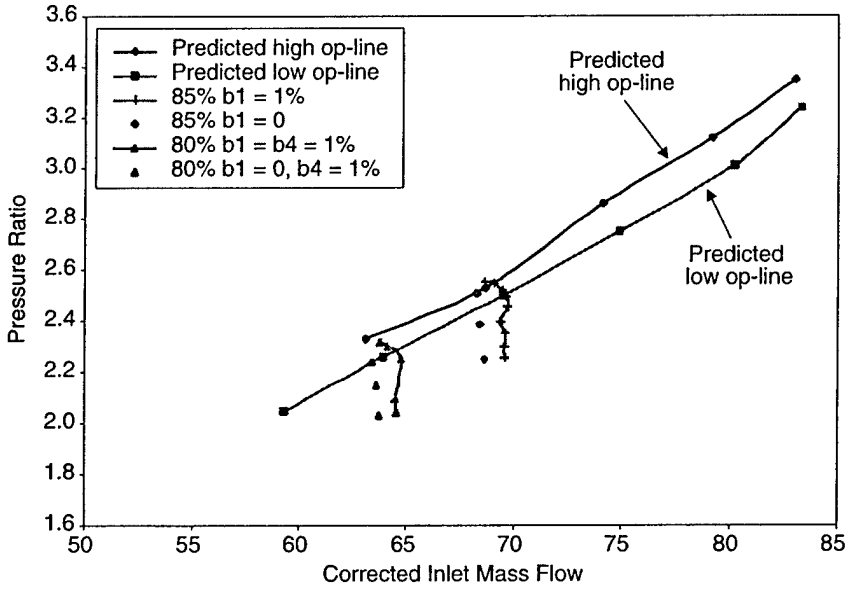

Figure 22: Effects of bleed at low operating speeds.

After safely achieving 85% speed, the bleeds were set to the known safe condition at 80%, (B1 = 1%, B4 = 1%, and B6 = 0) and a speedline was executed. Once stall was encountered, the normal procedure of opening the throttle did not bring the stage out of stall. To recover, all bleeds were re-opened and the stage began pumping. Prior to stalling, audible variations and slight increases in vibration levels were noted, provided clues that the stage was not operating as intended. All bleeds were reset (B1 = 1%, B4 = 1%, and B6 = 0), then B4 was closed. The audible noise was eliminated, and the vibration levels were reduced. The speedline was rerun and included in this report. A peak pressure ratio of 2.55 at 69 lb/s with an adiabatic efficiency of 87.6% was recorded.

Several points were also taken with the inlet boundary layer bleed off (B1 = 0); the effects can be seen in Figure 22. At similar pressure ratios the efficiency of the stage with inlet boundary layer bleed off is about 0.6% lower and the stage mass flow rate is reduced by about 1 lb/s. The bleed flow variations with inlet mass flow are collected in Figure 23.

Discussion

The predictions in the 75-85% operating range show good agreement for pressure ratio and mass flow, and the rotor exhibits crisp well defined stall characteristics. Recovery from stalls

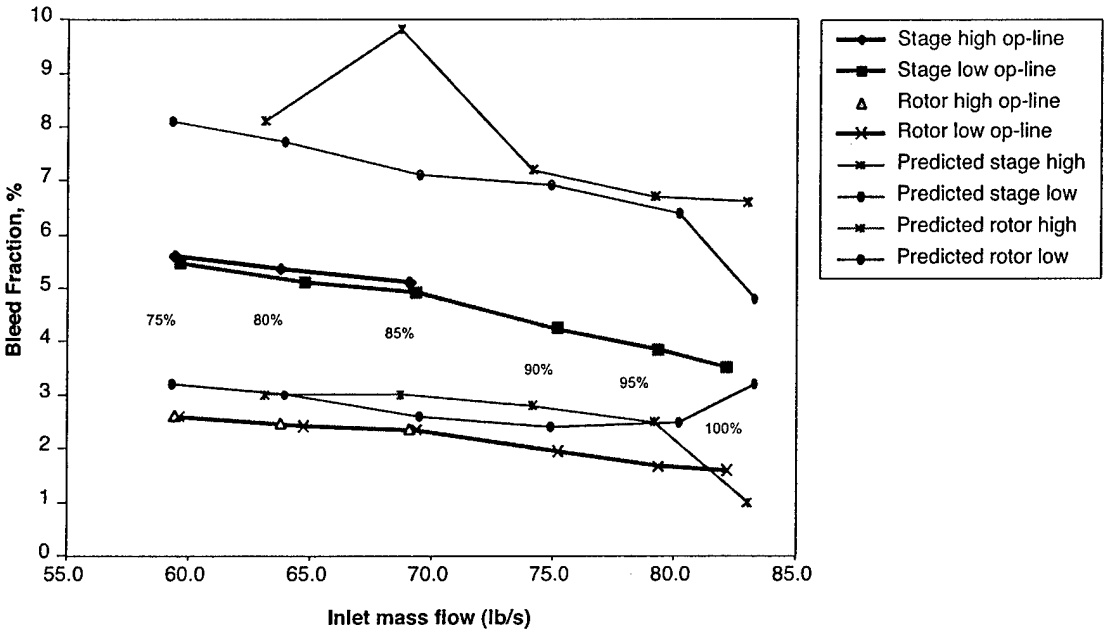

Figure 23: Variation of bleed flows with inlet mass flow for various conditions.

induced during low starting bleed rates at both 80 and 85% speed required all bleeds to be opened, simply reducing backpressure on the stage was insufficient to bring the stage out of stall.

At 75 and 80% of design speed, the rotor operated in a hub critical mode (blade sections close to the hub stalled first), and some starting bleed at the hub was required to stabilize the stage. At 85% and above, the rotor became tip critical (blade sections closer to the tip stalled first), and hub starting bleeds were required. The predicted high operating line is almost identical to the stall line as evidenced by our test experience.

90, 95 and 100% Speedlines

Based upon the experiences at lower speeds, and the desire to reduce the risk of mechanical damage to the rotor at these higher speeds, the rotor was mapped only from choke to the low operating line predicted pressure ratio. The only bleed configuration was B1 = 0, B4 = 0, and B6 = 0 which matched the predicted stage performance configuration.

As seen in the map, the characteristics were vertical for these speeds. The predicted mass flows were slightly higher than measured, which may be attributed to the stage bleed rates being lower than predicted.

At 90% speed, a pressure ratio of 2.76, at 75.2 lb/s with an adiabatic efficiency of 85.1% were recorded. This measured low operating line point matches exactly to predicted pressure ratio and inlet mass flow. The measured stage total bleed rate was about 4%, vs a predicted 7% Figure yy.

At 95% speed a pressure ratio of 2.99, at 79.3 lb/s with an adiabatic efficiency of 82.8% were recorded. The pressure ratio agrees well with predictions, while the mass flow is 0.8 lb/s lower than predicted. The measured stage total flow rate was again about 3% lower than the prediction.

At 100% speed a pressure ratio of 3.17, at 82.1 lb/s with an adiabatic efficiency of 78.7% were recorded. At this speed, we observed the greatest divergence in measured stage mass flow vs prediction, 1.2 lb/s. The pressure ratio obtained does fall on the predicted lower operating line. The measured stage total bleed rate was 3.5% vs. a predicted 4.8%.

Discussion

The predictions show that at the 100% design condition, the rotor predicted bleed rate is 1%, and the stage is nearly 7%. The trends experienced during testing support the rotor predicted

bleed rate of 1%, but not the stage total bleed rate. It appears that the stage total bleed rate would be around 3.5% if the stage were to be operated at the higher operating line conditions.

Post test inspection of the rotor revealed that the composite winding was generally in satisfactory condition. The labyrinth teeth showed minimal if any wear, and the rub areas revealed narrow, well defined contact areas.

CONCLUSIONS

This program, comprising the design, analysis and test of a very high pressure compressor enabled by aspiration of the low energy viscous flows from diffusion-limiting locations on the surfaces of the flow path, leads us to the following conclusions:

1. Removal of the low energy flow in the amount of a percent or less does in fact enable an increase in low-loss diffusion, such as to approximately double the compressor work, as hypothesized.
2. The effects of aspiration are quantitatively represented by a computational MISES-based design system in which the aspiration is represented by a prescribed mass flux into the wall at the location of a slot or hole which provides the actual removal.
3. A three dimensional viscous analysis by APNASA yielded a performance prediction for the compressor stage which is very close to the experimentally observed performance.
4. The novel mechanical structure devised for the aspirated stage, including a rotor split fore and aft into two integrally bladed halves, with a graphite-polymer wound tip shroud, proved to be mechanically sound and expeditious for the purposes of the experiment.
5. Overall the program provides a sound technology base for the design of aspirated stages in which tip shrouds can be used for control of tip clearance effects and for bleed flow management.

REFERENCES

1. Kerrebrock, J. L., Drela, M., Merchant, A. A., and Schuler, B. J., "A Family of Designs for Aspirated Compressors," ASME Paper 98-GT-196, ASME IGTI Conference, June 1998.
2. Merchant, Ali A., Drela M., Kerrebrock, J. L., Adamczyk, J. J., and Celestina, M., "Design and Analysis of a High Pressure Ratio Aspirated Compressor Stage," ASME IGTI Conference, 2000-GT-619, June 2000.

3. Merchant, A. A., "Design and Analysis of Axial Aspirated Compressor Stages", PhD thesis, MIT, Cambridge MA, June 1999.
4. Youngren, H.H. and Drela, M., "Viscous/Inviscid Method for Preliminary Design of Transonic Cascades," AIAA Paper AIAA-91-2364, 1991.
5. Adamczyk, J.J., "Model Equation for Simulating Flows in Multistage Turbomachines," *ASME J. Turbomachinery*, 103(2), 1985, pp. 430-437.
6. Schuler, B. J., Kerrebrock, J. L. and Merchant, A., "Experimental Investigation of an Aspirated Fan Stage," ASME Paper GT-2002-30370, 2002 IGTI Conference, Amsterdam, the Netherlands, June, 2002; see also Schuler, B.J., "Experimental Investigation of an Aspirated Fan Stage", PhD Thesis, MIT, Cambridge MA, June 2001.
7. Bollapragada, S., Presentation at Engineering Design Review, June 2000.